Adsorbed species and reaction rates for NO–CO–O_2 over Rh(111)

H. Permana and K.Y. Simon Ng

Wayne State University, Department of Chemical Engineering, Detroit, MI 48202, USA

Charles H.F. Peden

Environmental Molecular Sciences Laboratory, Pacific Northwest National Laboratory, Richland, WA 99352, USA*

Steven J. Schmieg, David K. Lambert and David N. Belton ‡

Physics and Physical Chemistry Department, General Motors Research and Development Center, Warren, MI 48090-9055, USA

Received 14 January 1997; accepted 3 June 1997

We have studied the NO–CO–O_2 reaction over a Rh(111) catalyst by monitoring the reaction products (CO_2, N_2O, and N_2) and the infrared (IR) intensity of surface CO and NO at various partial pressures of NO, CO and O_2, and sample temperatures. The selectivity for N_2O formation, apparent activation energy for product formation, and NO consumption rate during NO–CO–O_2 are identical to those measured during the NO–CO reaction. The IR measurements show that during NO–CO–O_2 the same two adsorbed species, NO at 1640 cm^{-1} and linear CO at $\sim$ 2040 cm^{-1}, are present in the same surface concentrations as during NO–CO. For this reason the NO–CO–O_2 kinetics are dominated by the NO–CO kinetics, the NO consumption is rate limited by dissociation of adsorbed NO, and the N_2O selectivity is dominated by surface NO coverage. In contrast, O_2 consumption is adsorption rate limited with the NO–CO adsorption–desorption equilibrium controlling the vacant sites required to dissociatively adsorb O_2. These kinetic and IR data of the CO–NO–O_2 reaction and our interpretation of them agree with previous studies over supported Rh catalysts and thus confirm the previously proposed explanation. From RAIRS and kinetic data we estimate the rate constant for the CO + O $\rightarrow$ CO_2 elementary step. The pre-exponential factor for this rate is 2×10^{10} s^{-1}, a factor of 50 smaller than previous estimates. This rate constant is important to the NO–CO–O_2 kinetics because it affects O coverage, which, under certain conditions, inhibits NO consumption.

Keywords: NO, CO, O_2, Rh, kinetics, RAIRS

1. Introduction

The emission of nitrogen oxides (NOx) by automobiles is primarily controlled by reacting NOx with CO in a catalytic converter [1]. To a large extent a converter's NOx performance is determined by whether NO or O_2 oxidize the CO in the exhaust to CO_2. This competition is seen in the effect of O_2 on the kinetics of the NO–CO reaction. We have used kinetic measurements and reflectance absorption infrared spectroscopy (RAIRS) to study the CO–NO–O_2 reaction over Rh(111).

In a previous paper [2] we used the same techniques to study the NO–CO reaction over Rh(111). Here, we show that the addition of O_2 to the feed has little effect – our understanding of the NO–CO reaction also applies to the CO–NO–O_2 system. In previous studies of the NO–CO reaction at the elementary step level over Rh and Pt–Rh single crystals we found [2–7] the same three products (CO_2, N_2O, and N_2) and similar kinetics to the NO–CO reaction over supported Rh and Pt–Rh catalysts. Of the proposed NO–CO reaction mechanisms [8–14], we favored [2,4–7] the simplest:

$$CO(g) + S \rightleftharpoons CO(ad) \quad (1)$$

$$NO(g) + S \rightleftharpoons NO(ad) \quad (2)$$

$$NO(ad) + S \rightarrow N(ad) + O(ad) \quad (3)$$

$$CO(ad) + O(ad) \rightarrow CO_2(g) + 2S \quad (4)$$

$$NO(ad) + N(ad) \rightarrow N_2O(g) + 2S \quad (5)$$

$$N(ad) + N(ad) \rightarrow N_2(g) + 2S \quad (6)$$

In this paper we show that with one added step,

$$O_2(g) + S \rightleftharpoons 2O(ad) \quad (7)$$

this mechanism also explains the NO–CO–O_2 reaction over Rh(111).

There have been previous studies of the CO–NO–O_2 reaction over alumina-supported Pt and Rh catalysts [15–25]. One approach has been to investigate the effect of NO on CO–O_2 kinetics since until recently the NOx standard was easier to meet than the CO standard. Near

* Pacific Northwest National Laboratory is a multiprogram National Laboratory operated for the US Department of Energy by Batelle Memorial Institute under contract number DE-AC06-76RLO 1830.

‡ To whom correspondence should be addressed.

stoichiometry, even a small amount of NO inhibits the CO–O_2 reaction and the overall kinetics are dominated by the characteristics of the CO–NO reaction rather than the CO–O_2 reaction. However, since the current regulations impose much stricter NOx standards [26] we focus on the effect of O_2 on the NOx emissions.

2. Experimental

The experiments were performed in a moderate pressure (< 100 Torr: 1 Torr= 133.3 N m^{-2}) reactor coupled to an ultrahigh vacuum (UHV) analysis chamber. The reactor was equipped with a gas chromatograph (GC) and a Fourier transform IR spectrometer. The Fourier transform IR spectrometer was a Mattson RS-10000 with a water-cooled source. Details of the reactor system, gas handling methods, sample preparation and cleaning, GC measurements, and the spectrometer and the optical system were reported in our previous papers [2–7,27].

We operated the reactor as a flow reactor. In the gas phase, NO and O_2 react with well known kinetics [28]:

$$2NO + O_2 \rightarrow 2NO_2 ,$$

$$\frac{dNO}{dt} = kP_{NO}^2 P_{O_2}^1 .$$

Here P_{NO} and P_{O_2} are the partial pressures of NO and O_2, respectively. Previous experiments [23,24] with NO over Pd have encountered difficulties when this gas phase reaction produced enough NO_2 to significantly affect the overall reaction rates. We avoided this by using a flow reactor and limiting $P_{NO} < 4$ Torr. Gas phase NO_2 formation rates were calculated using the rate constant of Atkinson et al. [29]. Our reactor volume was 0.370 ℓ. Residence time in the reactor ranged from 260 to 2600 s. To limit NO_2 formation in the gas phase,

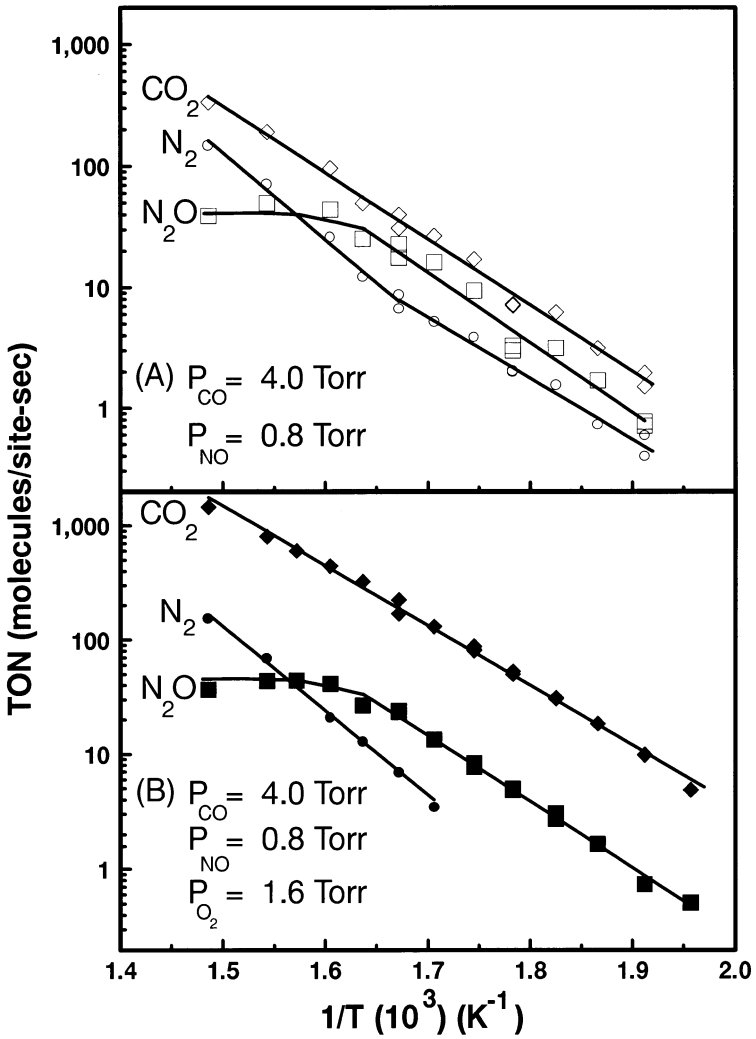

Figure 1. Specific rates of CO_2, N_2O, and N_2 formation for the NO–CO–O_2 reaction over Rh(111) as a function of $(1/T)$ using: (A) $P_{NO} = 0.8$ Torr, $P_{CO} = 4.0$ Torr and (B) $P_{NO} = 0.8$ Torr, $P_{CO} = 4.0$ Torr, $P_{O_2} = 1.6$ Torr.

we monitored the IR transmission spectra under flow conditions at room temperature and set the flow rates of CO, O_2, and NO so that no more than 0.2% of the NO reacted to form NO_2. Consequently, less than 1% of the products formed at reaction temperature were due to the reaction of NO_2 with CO.

Our IR spectra are averages of 1000 scans at 4 cm^{-1} resolution (taken in 2.5 min). Two methods [2] were used to obtain reflectance absorbance spectra: polarization spectroscopy (PS) and conventional RAIRS. The PS method shows only adsorbed species, without spectral interference from gas species. It is especially useful in the present experiment since there are four gas phase species (NO, CO, CO_2, and N_2O) that interfere with the adsorbed species.

We found that PS worked well from 1800 to 2200 cm^{-1}. However, the PS spectra had irreproducible features near the vibrational frequency of the adsorbed NO ($\sim$1600 cm^{-1}) of about 10^{-3} absorbance units. These artifacts were later found to be from an IR absorbing film on our ZnSe windows. The artifacts disappeared when the ZnSe windows were replaced by CaF_2 windows.

To avoid the spectral artifacts near 1600 cm^{-1} in the present experiments, we used conventional RAIRS. Even though RAIRS sees both gas phase and adsorbed species, adsorbed NO is well resolved from gas phase NO and N_2O. The reference spectra were taken with the cell evacuated to 10^{-8} Torr. To avoid RAIRS artifacts, we found that sample temperature T had to be the same for both the sample and reference spectra. However, others have reported that for their system, T during the reference spectrum did not affect the quality of their RAIRS data [30].

3. Results

3.1. Kinetic measurements

Figure 1 shows the measured turnover number (TON) in molecules/(site s) for the three products (CO_2, N_2O, and N_2) from the NO–CO (figure 1A) and NO–CO–O_2 (figure 1B) reactions over Rh(111). The NO–CO kinetic data in figures 1–4 have been reported previously [2,7]. The TON calculations were based on 1.67×10^{15} Rh sites/cm^2. All of the data were obtained under flow conditions as discussed in section 2. The data in figure 1 were all obtained with NO conversion below 15%. The low T limit, 523 K, was determined by the sensitivity of our GC. (We needed enough NO conversion to accurately measure the products.) The high T limit, 673 K, was set by the fact that this reaction is very exothermic. Thus, as the reaction rate increased with T, eventually the heat released by the reaction could not be compensated by our temperature controller. If T was raised above 675 K, then it jumped to $>$ 725 K within 2–5 s. Above 725 K the NO conversion was too high for us to operate in the low conversion limit. We could only measure N_2 TONs$>$ 8 molecules/(site s) with O_2 in the feed because our GC had poor sensitivity for N_2. Without O_2 in the feed, N_2 rates can be calculated from the ratio of N_2O to CO_2 and the known stoichiometry for N_2O and N_2 production. That is not possible in the CO–NO–O_2 reaction when CO_2 is formed by the simultaneous reaction of CO with both O_2 and NO.

The data in figure 1 show that CO_2 forms with an apparent activation energy of 25.0 kcal/mol over the entire T range regardless of whether O_2 is incorporated in the feed; however, the rate of CO_2 production (R_{CO_2}) increases by a factor $\sim$ 4 when O_2 is added. Also, N_2O and N_2 production rates are not affected by the addition of 1.6 Torr of O_2, which means that the NO consumption rate (R_{NO}) is independent of the presence of gas phase O_2 under our conditions. We calculate R_{NO} from:

$$R_{NO} = 2(R_{N_2} + R_{N_2O}), \tag{8}$$

where R_{N_2} and R_{N_2O} are the measured rates of N_2 and N_2O formation, respectively. This follows from the stoichiometry of the individual reactions:

$$2NO + CO \rightarrow N_2O + CO_2 \tag{9}$$

$$NO + CO \rightarrow \tfrac{1}{2}N_2 + CO_2 \tag{10}$$

Table 1 gives activation energies and prefactors that fit the measured rates.

Table 1
Values for E_a and C to calculate CO_2, N_2O, and N_2 formation rates over Rh(111) from the expression, TON = $C\exp(-E_a/RT)$. Values are given for two mixtures, with and without O_2

Rh(111)		CO_2	N_2O	N_2
P_{CO} = 4.0 Torr P_{NO} = 0.8 Torr P_{O_2} = 1.6 Torr	E_a (a)	24.0	26.3 <600K	*
			0 >600K	33.7
	C (b)	1.0×10^{11}	8.7×10^{10} <600K	*
			~40 >600K	1.4×10^{13}
P_{CO} = 4.0 Torr P_{NO} = 0.8 Torr	E_a (a)	25.0	26.6 <600K	23.2
			0 >600K	32.6
	C (b)	4.9×10^{10}	1.0×10^{11} <600K	2.3×10^{9}
			~40 >600K	6.6×10^{12}

(a) kcal/mol.
(b) molecules/(site s).
* Not measured.

Figure 2 shows the dependence of the TON on the partial pressure of CO (P_{CO}) both with and without gas phase O_2. With $P_{NO} = 0.8$ Torr and no O_2 (figure 2B), the reaction rate is zero order in P_{CO} for $P_{CO} < 5$ Torr and it shows a slight negative order behavior at $P_{CO} > 5$ Torr. Addition of O_2 does not alter R_{N_2} or R_{N_2O} (figure 2B), but does sharply increase R_{CO_2}. With oxygen present, R_{CO_2} shows -1/2 order kinetics over the entire P_{CO} range.

The P_{NO} dependence data for both reactions (with and without O_2) are shown in figure 3. Without oxygen at low P_{NO} (figure 3A), R_{N_2O} and R_{CO_2} are +1 order in P_{NO} and R_{N_2} is zero order in P_{NO}. Above ~ 1 Torr the reaction rate stabilizes and shows no dependence on P_{NO}. When 1.6 Torr of O_2 is added to the feed (figure 3B), R_{CO_2} increases by a factor of 4 and no longer shows any P_{NO} dependence. The addition of 1.6 Torr O_2 does not affect R_{N_2} or R_{N_2O}.

Figure 4 shows the P_{O_2} dependence with P_{NO} and P_{CO} fixed at 4 and 0.8 Torr, respectively. R_{CO_2} is +1 order in P_{O_2}. R_{N_2} is zero order in P_{O_2}. R_{N_2O} is zero order in P_{O_2} below 3 Torr and −0.6 order at higher P_{O_2}.

3.2. RAIRS measurements under reaction conditions

As discussed in section 2, we obtained IR spectra of the adsorbed species with PS for 1800–2200 cm^{-1} and with conventional RAIRS for 1200–1800 cm^{-1}. We have previously reported IR spectra of the adsorbed species on Rh(111) during the NO–CO reaction [2]. In the present study, independent of P_{O_2}, the spectral peaks occur at the same frequencies as in ref. [2]. Briefly, for all of the reaction conditions we observed, both with and without O_2, there is one broad surface feature near 1640 cm^{-1} due to adsorbed NO and one sharp feature at 2030–2050 cm^{-1} due to CO. Under reaction conditions, the full width at half maximum of the NO feature is ~ 100 cm^{-1}, larger than the 25–60 cm^{-1} width for NO on Rh(111) in UHV [2]. Under reaction conditions, from the width and shape of the observed peak, there must be at least three

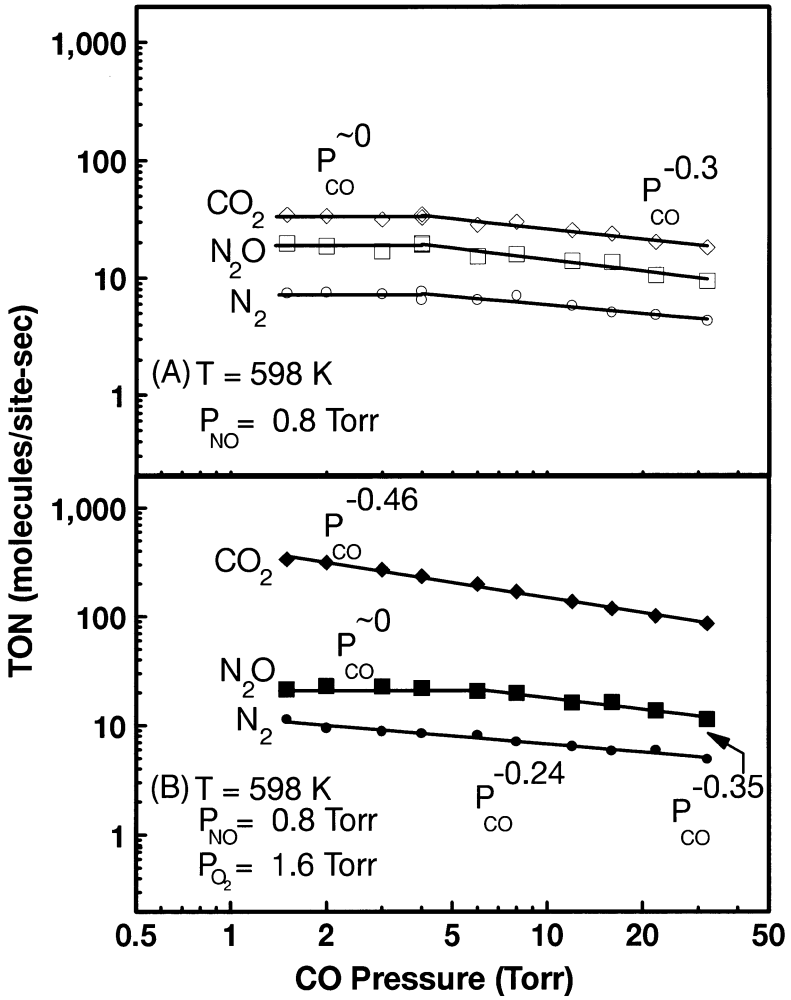

Figure 2. Effect of CO pressure on the specific rates for CO_2, N_2O, and N_2 formation for the NO–CO–O_2 reaction over Rh(111) using: (A) 0.8 Torr NO and (B) 0.8 Torr NO and 1.6 Torr O_2.

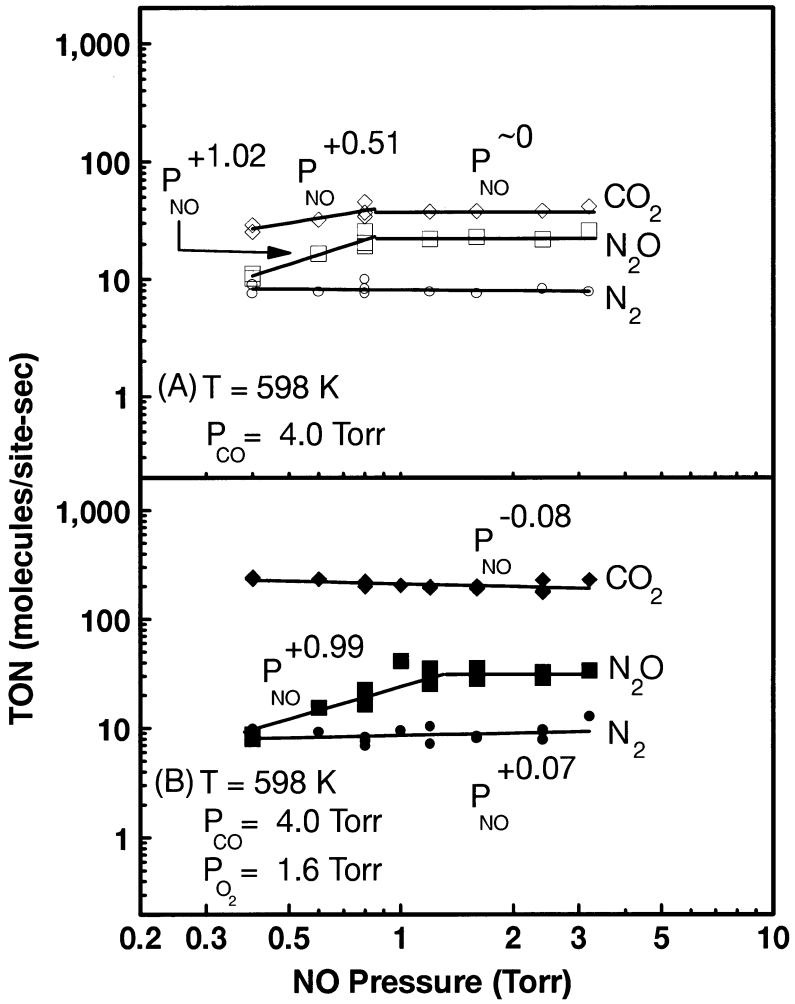

Figure 3. Effect of NO pressure on the specific rates for CO_2, N_2O, and N_2 formation for the NO–CO–O_2 reaction over Rh(111) using two different reaction conditions: (A) $P_{CO} = 4.0$ Torr and (B) $P_{CO} = 4.0$ Torr, $P_{O_2} = 1.6$ Torr.

spectral lines. As discussed in our previous paper [2], recent experiments suggest that all the NO is at three-fold hollow sites – the different vibrational frequencies are caused by different local environments. In the CO stretching region we detect only atop CO [2]. Even though our spectra extend to 4000 cm^{-1}, no surface species were detected above 2100 cm^{-1}. We have observed isocyanate on Rh(111) at ~ 2200 cm^{-1} in separate experiments, but it is below our detection limit for all the conditions reported here.

In figure 5 we plot the integrated IR intensities of bridge NO (A_{NO}, defined as the integrated area under all the NO peaks) and atop CO (A_{CO}), as functions of $1/T$. (This facilitates comparison with the kinetic data in figure 1.) The IR data can be compared directly with the kinetic data since the experimental conditions were the same. With $P_{CO} = 4$ Torr CO and $P_{NO} = 0.8$ Torr, A_{NO} decreases from 0.19 to 0.05 cm^{-1} as T increases from 548 to 673 K; over the same range, A_{CO} is constant at 0.04 cm^{-1} up to 573 K, increases sharply to 0.11 cm^{-1} as T increases to 623 K, and then decreases back to 0.08 cm^{-1} at 673 K. As O_2 is added to the feed, neither A_{NO} nor A_{CO} change significantly.

We have also obtained RAIRS data as functions of P_{CO}, P_{NO} and P_{O_2}, as shown in figure 6. As with the T-dependent data in figure 5, the RAIRS data with and without oxygen are indistinguishable (figures 6A and 6B) when P_{CO} and P_{NO} are varied. However, when P_{O_2} increases, A_{NO} decreases slightly and A_{CO} increases slightly.

4. Discussion

4.1. Review of NO–CO mechanism

We have previously studied the NO–CO reaction [2–7]. As discussed in section 1, we favor [2] the simplest proposed mechanism: formation of N_2 and N_2O via separate pathways. An alternative is that N_2 and N_2O are formed via a common intermediate. Our mechanism successfully explains kinetic data for the NO–CO reac-

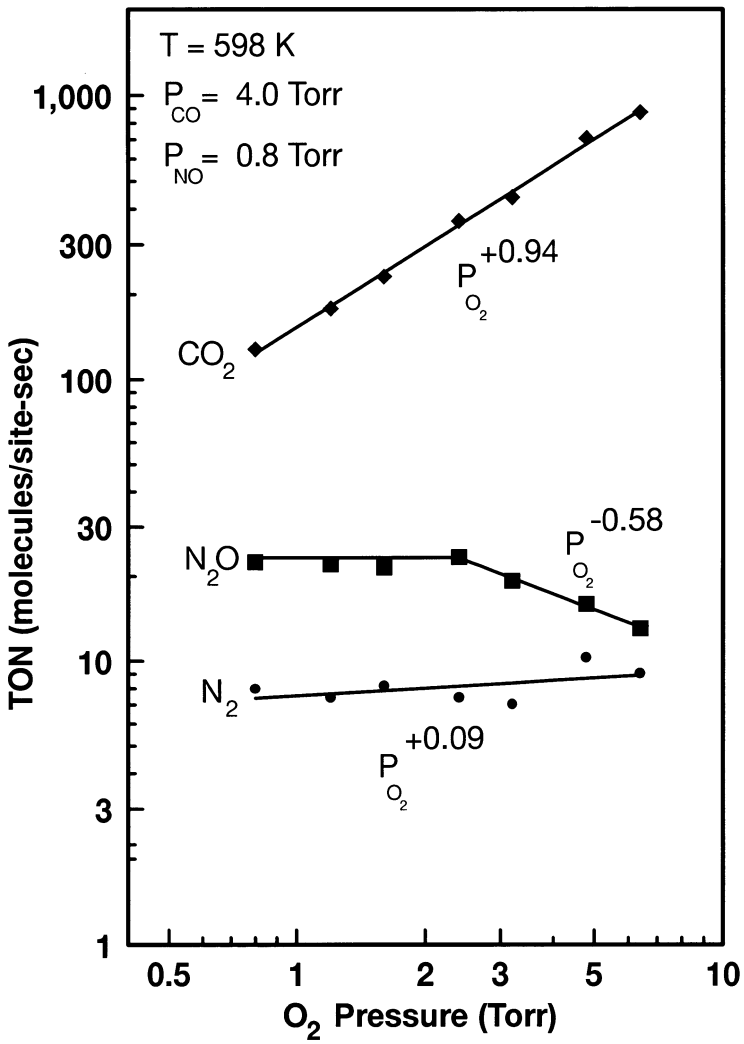

Figure 4. Effect of O_2 pressure on the specific rates for CO_2, N_2O, and N_2 formation for the NO–CO–O_2 reaction over Rh(111).

tion over Rh(111) in the NO pressure range from 0.4 to 40 Torr [2]; however, uncertainty in the rate constants for steps (3) and (5) limits our ability to prove it is the correct mechanism. Within this model, the rate expressions for steps (5) and (6) are:

$$R_{\text{form}}^{N_2O} = \theta_N \theta_{NO} \nu \exp\left(-\frac{E_a}{RT}\right), \tag{11}$$

$$R_{\text{form}}^{N_2} = \theta_N^2 \nu \exp\left(-\frac{(E_a - \alpha_N \theta_N)}{RT}\right). \tag{12}$$

In eqs. (11) and (12), θ_{NO} and θ_N are the coverages of NO and N, respectively, ν is the pre-exponential factor, E_a is the activation energy, and α_N is the dependence of E_a on θ_N. The RAIRS data that we recently reported [2], as well as those in the present paper, strongly support this model which predicts that N_2O formation is first order in θ_{NO} and that N_2 formation is dependent on θ_N but not on θ_{NO}.

Qualitatively, the primary feature of the NO–CO kinetics is the insensitivity of the N_2O selectivity to reaction temperature (500 K $\leqslant T \leqslant$ 700 K), CO pressure (1 Torr $\leqslant P_{CO} \leqslant$ 40 Torr) and NO pressure (1 Torr $\leqslant P_{NO} \leqslant$ 40 Torr). Under these conditions, RAIRS shows that θ_{NO} is quite high, and θ_{CO} is very low. Consequently, our model predicts that NO dissociation is the rate limiting step (RLS). The model also predicts that θ_N is on the order of 0.2 ML (monolayer) and N_2O production dominates over N_2 production. The RAIRS data shows that when $P_{NO} < 1$ Torr and $T > 600$ K, θ_{NO} drops, θ_{CO} increases, indicating that the selectivity of the reaction switches towards N_2 production. Within this model it is precisely the surface coverage of NO that controls the selectivity for N_2O (S_{N_2O}) as well as the overall reaction rate which is equivalent to R_{CO_2}. R_{CO_2} is dependent on θ_{NO} because the NO dissociation rate ($R_{NO\,diss}$), which determines the rate at which O atoms are supplied for CO_2 formation, depends on both θ_{NO} and θ_V, the vacant site coverage. As has been previously reported [31,32], $R_{NO\,diss}$ is strongly dependent on θ_V and thus

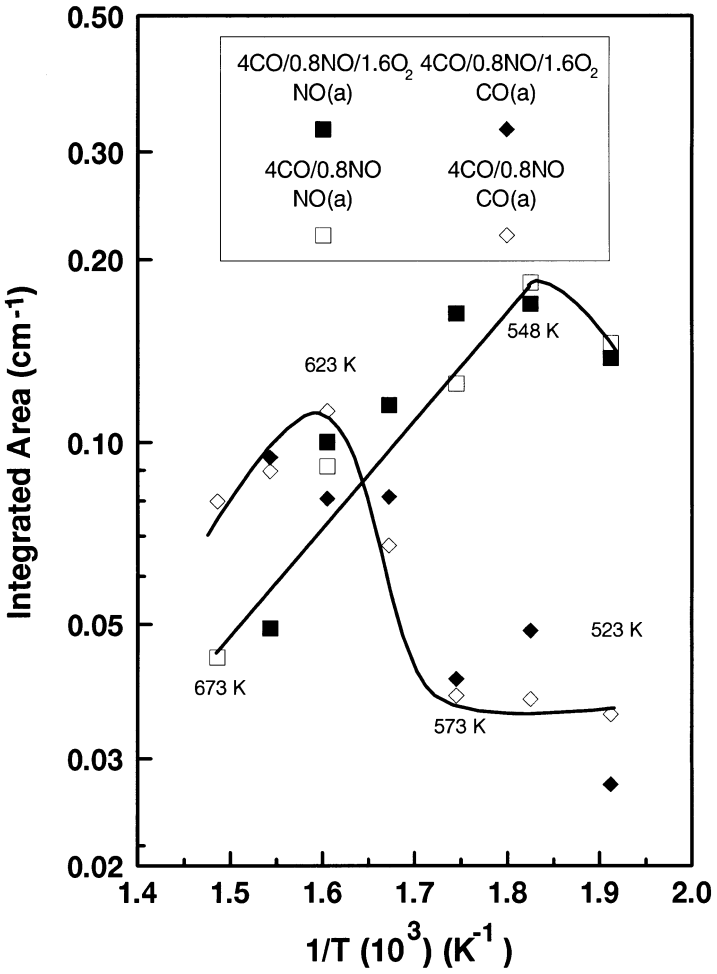

Figure 5. Integrated intensities of surface NO and CO peaks from figure 1 as a function of $(1/T)$. The open symbols are for 4.0 Torr CO/0.8 Torr NO and the closed symbols are for 4.0 Torr CO/0.8 Torr NO/1.6 Torr O_2.

changes in surface coverage can lead to large changes in the $R_{NO\,diss}$.

4.2. $NO–O_2$ competition in a stoichiometric mixture

Our objective was to understand the effect of O_2 on the NO–CO reaction. Figures 1–4 show the kinetic data that we obtained to achieve this understanding. We are careful to note two important conditions of our experiment. First, T is below the 600°C maximum typical for supported catalyst work [15,17,19–22]. Second, the conversions are low – we do not examine conditions where one reactant is consumed.

The Arrhenius behavior (figure 1) shows that when a stoichiometric amount of O_2 (1.6 Torr) is added to a feed with $P_{CO} = 4$ Torr and $P_{NO} = 0.8$ Torr, the NO consumption rate R_{NO} is unchanged over the range of T we examine. This is evidenced by the fact that neither R_{N_2O} nor R_{N_2} are changed by adding O_2. Consequently, S_{N_2O} is also unaffected by O_2 incorporation. Based on our model of the NO–CO reaction we conclude that addition of the gas phase O_2 had no effect on θ_{NO}, θ_{CO} or θ_V. The RAIRS data taken with and without 1.6 Torr O_2 also indicate that θ_{NO} and θ_{CO} are unaffected by O_2 addition. As figure 5 shows, A_{NO} and A_{CO} during NO–CO and NO–CO–O_2 are indistinguishable by RAIRS. In our previous paper [2], we showed that $A_{NO} \propto \theta_{NO}$ up to about 0.6 saturation θ_{NO}. A similar relationship holds for CO. Since both A_{NO} and A_{CO} are unaffected by O_2 addition we conclude that θ_{NO} and θ_{CO} are also; consequently O_2 addition does not significantly change θ_V. This is consistent with the fact that $R_{NO\,diss}$, which is equal to R_{NO} and depends on both θ_{NO} and θ_V [31,32], is unaffected by O_2 addition (figure 1).

The addition of 1.6 Torr of O_2 does increase R_{CO_2} by a factor of ~ 4. All of the CO_2 formed by the NO–CO reaction comes from NO consumption, but $\sim 80\%$ of the CO_2 formed by the NO–CO–O_2 reaction comes from O_2 consumption. In the stoichiometric NO–CO–O_2 mixture, the gas phase O atom ratio to O_2 is 0.8; therefore, NO and O_2 oxidize CO in roughly the gas phase O atom ratio. In other words, at the stoichiometric point, gas phase NO and gas phase oxygen appear to have *equal*

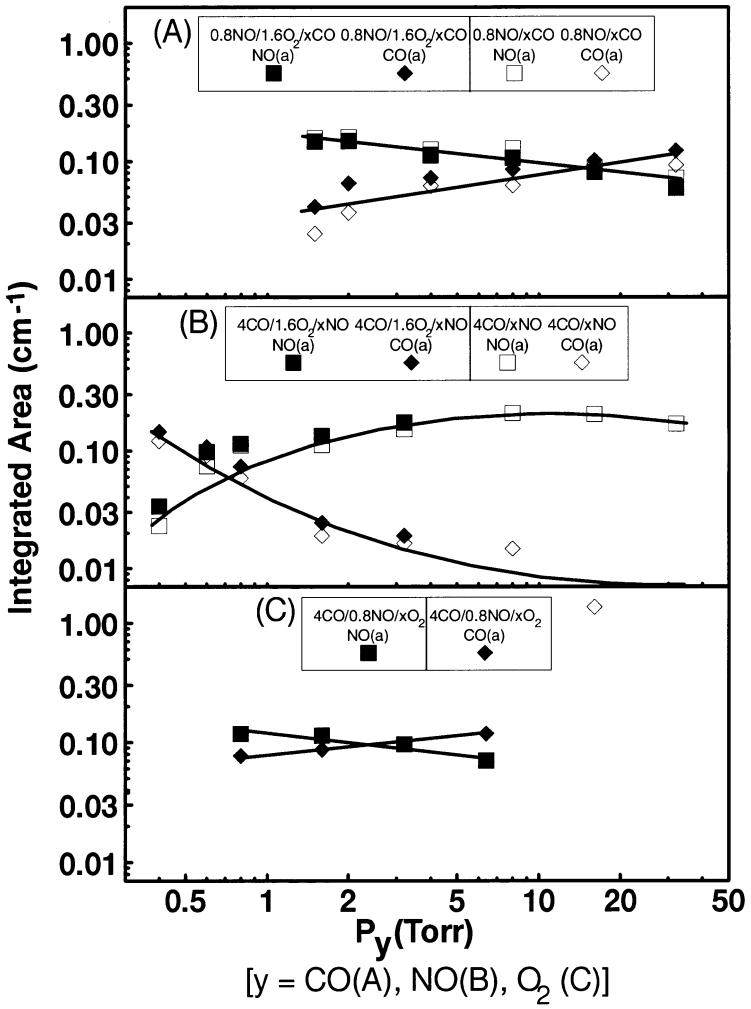

Figure 6. Integrated intensities for the CO and NO peaks as a function of: (A) CO pressure, (B) NO pressure, and (C) O_2 pressure at 598 K.

power as oxidants over Rh(111) in this temperature regime. Actually, at these pressures and temperatures, the competition is between *gas phase* O_2 and *surface* NO. This follows from the RAIRS data in figures 5 and 6 that show that over our T range θ_{NO} is reasonably high under all conditions and $\theta_{NO} + \theta_{CO} \sim 1$. Thus, the RLS for O_2 consumption is adsorption (O_2 dissociation is much faster than O_2 desorption [10]), but the RLS for NO consumption is dissociation of adsorbed NO. Under conditions where O_2 adsorption is rate limiting we would expect θ_O to be quite low. Low θ_O is inferred from two experimental observations. First, it has been reported [33] that addition of even small amounts of surface O gives rise to an NO band at 1840 cm^{-1} that we do not see when O_2 is added to the gas phase. Second, adsorbed O increases the NO desorption rate [34] which would tend to lower θ_{NO}. Figure 5 shows that there is no change in θ_{NO} when O_2 is added to the gas phase. These two observations suggest that $\theta_O < 0.1$ ML. We conclude that NO and oxygen compete to react with CO under our conditions because of NO's strong ability to molecularly adsorb and block the vacant sites required for dissociative O_2 adsorption.

This delicately balanced competition between *surface* NO and *gas phase* O_2 is only found below $\sim$ 700 K with $P_{NO} = 0.8$ Torr. With $T > 700$ K the NO desorption rate becomes comparable to the NO flux and the surface "cleans up". This is seen in our RAIRS data where above 623 K, θ_{NO} and θ_{CO} are falling simultaneously. We predict steady-state θ_{NO} will fall below 0.1 ML at about 770 K by assuming an NO sticking coefficient of 1, our NO desorption rate constant [31], and assuming that product generation rates are slow compared to the adsorption/desorption rates (if they are not, the predicted T is lower). Once θ_{NO} is relatively low, sufficient vacant sites are available for both adsorption and dissociation of either NO or O_2. At higher T the competition between the oxidants depends upon the ratio of the desorption rate to the dissociation rate for each. Under these conditions we predict O_2 will dominate over NO for the following reasons: dissociation and desorption of molecularly bound O_2 both have quite low E_a and both

are very fast even at low temperature [31]. Reasonable estimates based on TPD data [34] suggest that both O_2 desorption and dissociation have similar rate constants of $\sim 10^{11}$ s^{-1} at 700 K. Thus, about half of the O_2 that sticks desorbs and half dissociates. For NO however, the situation is different. The E_a for both NO desorption and NO dissociation are large with E_a for desorption (29.7 kcal/mol) being significantly higher than that for dissociation (17.5 kcal/mol) [31]. Thus, whereas at low temperature NO dissociation predominates, above ~ 600 K (depending on θ_{NO} and θ_V) this situation reverses. For instance, by 760 K, the rate constant for NO desorption is approximately ten times that for dissociation [31]. Thus only about 10% of the NO that adsorbs on the surface is dissociated (at these temperatures and pressures, θ_V is large), whereas 50% of the oxygen dissociates. This implies that for $T > 700$ K, O_2 should be a much more powerful oxidant than NO. Unfortunately, as explained in section 2, our reactor could not be used to check this.

4.3. NO–O_2 competition in non-stoichiometric mixtures

We have shown that under relatively low temperature stoichiometric conditions, NO competes effectively with O_2 as the oxidant for CO; however, the exhaust streams which practical automotive catalysts encounter can be non-stoichiometric mixtures. The pressure-dependent kinetic measurements in figures 2–4 address this non-stoichiometric activity by systematically varying the concentrations of each reactant. Kinetic data obtained during the variation of P_{CO} (figure 2) show that without O_2, both R_{NO} and S_{N_2O} are fairly insensitive to P_{CO} but decrease slightly at $P_{CO} > 4$ Torr. In this pressure range, RAIRS (figure 6A) shows that surface CO replaces surface NO as P_{CO} is increased. Moreover, RAIRS shows no effect of gas phase O_2 on either the integrated intensities or any of the peak frequencies. Therefore, gas phase O_2 does not disturb this NO–CO competition. These data are in complete agreement with the kinetic data (figure 2) which show no change in R_{N_2O} and R_{N_2}. Thus, as we conclude in section 4.1, addition of 1.6 Torr O_2 in the feed ($\theta_O < 0.1$ ML) does not significantly alter θ_{NO}, θ_{CO} or θ_N.

As discussed in section 4.1, adding 1.6 Torr O_2 to the CO–NO feed increases R_{CO_2} by a factor of ~ 4 because gas phase O_2 reacts with CO to make $\sim 80\%$ of the CO_2. As shown in figure 2, $R_{CO_2} \propto P_{CO}^{-0.46}$ during the CO–NO–O_2 reaction. This effect is weaker than the $R_{CO_2} \propto P_{CO}^{-1}$ dependence observed for the CO–O_2 reaction and shows that gas phase NO moderates CO's inhibiting effect on O_2 consumption. The reasons for the moderation of CO inhibition can be understood using the RAIRS data. Figure 6A shows that as P_{CO} is raised θ_{NO} decreases and θ_{CO} increases. Swapping of NO for CO on the surface offsets the θ_V change so that $(d\theta_V/dP_{CO})$ is smaller for CO–NO–O_2 than it is for CO–O_2. When P_{CO} is raised during the CO–O_2 reaction, θ_V falls as first order in P_{CO} as θ_{CO} rises giving the P_{CO}^{-1} dependence in the reaction rate [10]. For CO–NO–O_2, the $P_{CO}^{-0.46}$ kinetics suggest a complex interplay of θ_{NO} and θ_{CO} with θ_V; however, qualitatively it is clear that over this entire P_{CO} range, incorporation of O_2 in the feed does not affect the essential NO–CO interplay on the surface.

The P_{NO}-dependent data solidify the picture put forth above. Over the entire P_{NO} range we examined, oxygen addition has no effect on R_{N_2O} and R_{N_2}. Also as before, addition of oxygen increases R_{CO_2} as gas phase O_2 dissociatively adsorbs at available vacant sites and then reacts with adsorbed CO. It is interesting to note the differences between the P_{NO} dependence and the P_{CO} dependence. In figure 2, for CO–NO–O_2, $R_{CO_2} \propto P_{CO}^{-0.46}$ out to $P_{CO} = 40$ Torr. In contrast, for CO–NO in figure 3, $R_{CO_2} \propto P_{NO}^{0}$ above 1 Torr both with and without O_2. Both the CO–NO and the CO–NO–O_2 data sets suggest that θ_{NO} saturates at $P_{NO} = 1$ Torr and as a consequence, θ_V stabilizes at this pressure; however, it is also possible that small changes in θ_{NO} and θ_V cancel to give no change in the reaction rate. Because RAIRS is insensitive to θ_{NO} changes when θ_{NO} is near saturation, IR data cannot resolve this issue. However, with O_2 present in the gas phase, R_{CO_2} is an extremely sensitive measure of θ_V (recall that O_2 consumption is adsorption limited and thus $\propto \theta_V^1$). Because $R_{CO_2} \propto P_{NO}^{0}$, we conclude that $\theta_V \propto P_{NO}^{0}$ also and increasing P_{NO} does not affect θ_{NO} ($0.3 < P_{NO} < 40$ Torr). This behavior is markedly different from that of CO during CO–O_2: $\theta_V \propto P_{CO}^{-1}$ up to $P_{CO} \approx 200$ Torr, at lower T where θ_{CO} would be much higher [10].

Why does CO inhibit the O_2 consumption reaction more strongly than NO? One possibility is that CO and O_2 compete for the same initial adsorption site. (On Rh(111), CO adsorbs at atop sites but NO adsorbs at three-fold hollow sites [2]). This simple argument however, ignores the steric hindrance of adsorbates at neighboring sites. Three-fold NO does block atop CO [33]. The CO–O_2 reaction also runs slower with NO in the feed (and on the surface) than without [35]. A second possibility is that θ_{NO} saturates and leaves a fixed, low number of vacant sites available for O_2 adsorption, but θ_{CO} does not stop increasing. This possibility was tested with a kinetic model that included a mobile precursor for NO adsorption [35]. In this model, above about 90% of saturation the sticking coefficient drops so fast that the coverage cannot significantly increase at these pressures. The available information suggests that the NO and CO sticking coefficients govern whether they exhibit negative order or zero order kinetics at high pressures.

Finally, we discuss the P_{O_2} dependence of the reaction. The CO_2 formation rates are easily understood in terms of adsorption limited O_2 consumption through a single initial adsorption site. The reasons for these +1 order kinetics are the same as for the CO–O_2 reaction [10]. Within this model, doubling P_{O_2}, doubles the

adsorption rate, which in turn doubles θ_O and ultimately doubles R_{CO_2}. Typical estimates for the steady-state O coverages under CO–O_2 conditions have been low. For instance the CO–O_2 model of Oh et al. [10] predicts that $\theta_O \approx 10^{-5}$ ML at 500 K with $P_{CO} = P_{O_2} = 8$ Torr. However, if the pre-exponential for the $CO + O \rightarrow CO_2$ step is also allowed to vary, the reaction rate data fit their model with $10^{-7} \leqslant \theta_O \leqslant 10^{-2}$. Our data provides additional information about the uncertainty in the rate constant for $CO + O \rightarrow CO_2$ and thus the steady state O coverages present under reaction conditions. In figure 4, R_{N_2O} and R_{N_2} are independent of P_{O_2} for $P_{O_2} < 2$ Torr. These results strongly suggests that θ_O, which is increasing to drive up R_{CO_2}, is still too low to appreciably affect θ_N and θ_{NO}. However, for $P_{O_2} > 2$ Torr R_{N_2O} is moderately negative order in P_{O_2}. Our RAIRS data (figure 6C) show a slight decline in A_{NO}, indicating that θ_{NO} is falling, which is in good agreement with the observation that R_{N_2O} is falling. The decline in θ_{NO} almost certainly is caused by an increase in θ_O. Previous UHV work has shown a strong interaction between surface O and NO [33,34]. Root et al. [34] showed θ_O need only be ~ 0.1 ML in order to decrease the NO desorption temperature by 45 K. Applying this 45 K temperature difference to reaction occurring at 598 K predicts a factor 10 increase in the NO desorption rate [1]. Assuming that this O–NO interaction causes θ_{NO} to fall when $P_{O_2} > 2$ Torr, that $\theta_O \approx 0.1$ ML, and that $\theta_{CO} \approx 0.125$ ML (based on A_{CO} in figure 6), we estimate that k for the CO_2 formation step is 6.8×10^4 s^{-1}. Because of uncertainty in the coverages, k could be as low as 3.4×10^4 s^{-1} or as high as 2.6×10^5 s^{-1}. This rate for the CO + O elementary step is within, but at the low end of the range that Oh [10] concluded was reasonable. The rate is important to CO–NO–O_2 kinetics because NO desorption and dissociation rates depend strongly on θ_O. In addition, in the limit of high P_{O_2} and low P_{CO}, the reaction is poisoned by the build-up of oxygen and the eventual oxidation of the surface.

To summarize the kinetic behavior, under low temperature conditions (< 700 K) with mixtures near stoichiometric, the addition of gas phase O_2 increases the CO_2 formation rate without affecting the NO consumption rate or the N_2O selectivity. Our RAIRS data clearly demonstrates that under these conditions, θ_{NO} and θ_{CO} are unaffected by P_{O_2}. However, when P_{O_2} is increased to about twice the stoichiometric amount, inhibition of the CO–NO reaction is observed. This inhibition pushes down R_{N_2O} with a $P_{O_2}^{-0.6}$ dependence. More significant for practical automotive catalysts is the fact that CO consumption is $P_{O_2}^{+1}$ dependent under these non-stoichiometric conditions and thus the reductant in the system is consumed much more rapidly by O_2 than by NO.

[1] Assuming $\nu = 10^{13}$ s^{-1} for both desorption states results in a 2.8 kcal/mol difference in E_a for the states, which gives a 10× rate difference at 598 K.

4.4. NO–CO–O_2: comparison to supported catalysts

Comparison to supported systems is an important check on the applicability of single-crystal catalyst work. Over Pt-containing catalysts, the reaction has been studied by Voltz et al. [17]. Their results are similar to those of Oh and Carpenter for Rh/Al_2O_3 catalysts [20]. Our results and conclusions for Rh(111) are in remarkably good agreement with those from the supported catalysts [20]. For instance, Oh and Carpenter [20] found that during the CO–NO–O_2 reaction: (1) the majority of the CO is consumed by reaction with O_2 (differences in concentrations used make a more quantitative comparison difficult), (2) E_a for CO–NO–O_2 is the same as for CO–NO, (3) CO consumption is +1 order in P_{O_2} (figure 4), (4) CO_2 formation is weakly negative order in P_{CO} (figure 2), (5) addition of NO to a CO–O_2 feed results in a suppression of the CO consumption rate (CO–O_2 rates are not reported here, but we have measured CO consumption to be a factor of 4 lower for CO–NO–O_2 than for CO–O_2), and (6) CO consumption is positive order at low P_{NO} changing to zero order at higher P_{NO} (figure 3).

Oh and Carpenter's [20] interpretation of their results is virtually identical to the explanation we put forth in sections 4.1 and 4.2. Although these authors did not have IR data during the NO–CO–O_2 reaction, they concluded that the surface must contain the same species as during NO–CO reaction because the light-off temperatures and kinetics were so similar to those for NO–CO (exactly as we observe here). Based on inferences to other IR studies they concluded that NCO was not responsible for the inhibition of $CO \rightarrow CO_2$ that they observed and our results here indicate that NCO is not an important surface species in the limit of large Rh particles. Finally, they ruled out the possibility that a CO–NO–O_2 feed leads to oxidation of the Rh particles. Considering that there is no evidence for oxidation of our single crystal and we see similar kinetics to the Rh/Al_2O_3 catalyst, we are in agreement with this conclusion also. In summary, there is remarkably good agreement between our Rh(111) results and those over Rh/Al_2O_3 catalysts. The RAIRS data we report here support the earlier conclusions by Oh and Carpenter that the NO–CO kinetics and surface species are dominant in determining the NO–CO–O_2 reaction kinetics.

5. Conclusions

We have examined the NO–CO–O_2 reaction over a Rh(111) catalyst under the following reaction conditions: $0.4 \leqslant P_{NO} \leqslant 32$ Torr, $0.8 \leqslant P_{CO} \leqslant 32$ Torr, $0.8 \leqslant P_{O_2} \leqslant 32$ Torr, and $525 \leqslant T \leqslant 675$ K. Our RAIRS data show that surface NO and CO coverages are unaffected

by the addition of stoichiometric amounts of O_2 to an NO–CO feed. Under these conditions O_2 consumption is adsorption limited with the necessary vacant sites controlled by the NO–CO adsorption–desorption equilibrium. NO consumption and the N_2O selectivity are not altered by addition of stoichiometric O_2 amounts. At P_{O_2} twice the stoichiometric amount, subtle effects on the N_2O formation rates are observed. Our RAIRS data suggests that N_2O formation falls in response to a decline in θ_{NO}. This interpretation and our kinetic data are in good agreement with previously published results over Rh/Al_2O_3 catalysts. As a final point, based on RAIRS and kinetic data we estimate the rate constant for the $CO + O \rightarrow CO_2$ elementary step. It is ~ 50 times smaller than the previously employed value, although consistent with previous estimate (10). This shows that the steady-state O atom concentrations on Rh surfaces are higher than previously thought. The improved rate constant will aid CO–NO–O_2 kinetic models.

Appendix. Kinetic parameters

A_{CO} = integrated IR intensity under CO peak
A_{NO} = integrated IR intensity under NO peak
dNO/dt = change in NO concentration with respect to change in time
$d\theta_V/dP_{CO}$ = change in vacant site coverage with respect to change in CO partial pressure
ν = pre-exponential factor
E_a = activation energy
α = dependence of E_a on θ_N
θ_N = surface coverage of N
θ_{NO} = surface coverage of NO
θ_V = vacant site coverage
θ_O = surface coverage of O
k = reaction constant
S_{N_2O} = N_2O selectivity
P_{NO} = partial pressure of NO
P_{O_2} = partial pressure of O_2
P_{CO} = partial pressure of CO
R_{NO} = rate of NO consumption
R_{N_2} = $R_{form}^{N_2}$ = rate of N_2 formation
R_{N_2O} = $R_{form}^{N_2O}$ = rate of N_2O formation
R_{CO_2} = rate of CO_2 formation
$R_{NO\,diss}$ = rate of NO dissociation

References

[1] K.C. Taylor, Catal. Rev. Sci. Eng. 35 (1993) 457.
[2] H. Permana, K.Y.S. Ng, C.H.F. Peden, S.J. Schmieg, D.K. Lambert and D.N. Belton, J. Catal., submitted.
[3] D.N. Belton and S.J. Schmieg, J. Catal. 138 (1992) 70; 144 (1993) 9.
[4] D.N. Belton, C.L. DiMaggio and K.Y.S. Ng, J. Catal. 144 (1993) 273.
[5] K.Y.S. Ng, D.N. Belton, S.J. Schmieg and G.B. Fisher, J. Catal. 146 (1994) 394.
[6] C.H.F. Peden, D.N. Belton and S.J. Schmieg, J. Catal. 155 (1995) 204.
[7] H. Permana, K.Y.S. Ng, C.H.F. Peden, S.J. Schmieg and D.N. Belton, J. Phys. Chem. 99 (1995) 16344.
[8] W.C. Hecker and A.T. Bell, J. Catal. 84 (1983) 200.
[9] A.A. Chin and A.T. Bell, J. Phys. Chem. 87 (1983) 3700.
[10] S.H. Oh, G.B. Fisher, J.E. Carpenter and D.W. Goodman, J. Catal. 100 (1986) 360.
[11] S.B. Schwartz, G.B. Fisher and L.D. Schmidt, J. Phys. Chem. 92 (1988) 389.
[12] C.H.F. Peden, D.W. Goodman, D.S. Blair, P.J. Berlowitz, G.B. Fisher and S.H. Oh, J. Phys. Chem. 92 (1988) 1563.
[13] B.K. Cho, B.H. Shanks and J.E. Bailey, J. Catal. 115 (1989) 486.
[14] B.K. Cho, J. Catal. 138 (1992) 255.
[15] J.H. Jones, J.T. Kummer, K. Otto, M. Shelef and E.E. Weaver, Env. Sci. Technol. 5 (1971) 797.
[16] G.L. Bauerle, G.R. Service and K. Nobe, Ind. Eng. Chem. Prod. Res. Develop. 11 (1972) 54.
[17] S.E. Voltz, C.R. Morgan, D. Liederman and S.M. Jacob, Ind. Eng. Chem. Prod. Res. Develop. 12 (1973) 294.
[18] G.B. Fisher, S.H. Oh, C.L. DiMaggio and S.J. Schmieg, in: *Proc. 9th Int. Congr. on Catalysis*, Vol. 3, eds. M.J. Phillips and M. Ternan (Chem. Inst. Canada, Ottawa, 1988) p. 1355.
[19] S.H. Oh and J.E. Carpenter, J. Catal. 98 (1986) 178.
[20] S.H. Oh and J.E. Carpenter, J. Catal. 101 (1986) 114.
[21] G. Leclercq, C. Dathy, G. Mabilon and L. Leclercq, in: *Catalysis and Automotive Pollution Control II*, ed. A. Crucq (Elsevier, Amsterdam, 1991) p. 181.
[22] J.L. Duplan and H. Praliaud, in: *Catalysis and Automotive Pollution Control II*, ed. A. Crucq (Elsevier, Amsterdam, 1991) p. 667.
[23] G.W. Graham, A.D. Logan and M. Shelef, J. Phys. Chem. 97 (1993) 5446.
[24] G.W. Graham, A.D. Logan and M. Shelef, J. Phys. Chem. 98 (1994) 1746.
[25] R. Burch, P.J. Millington and A.P. Walker, Appl. Catal. B 4 (1994) 6.
[26] J.G. Calvert, J.B. Heywood, R.F. Sawyer and J.H. Seinfeld, Science 261 (1993) 37.
[27] G.B. Fisher and S.J. Schmieg, J. Vac. Sci. Technol. A 1 (1983) 1064.
[28] D.M. Yost and H. Russell, *Systematic Inorganic Chemistry of the Fifth-and-Sixth-Group Nonmetallic Elements* (Oxford University Press, London, 1946).
[29] R. Atkinson, D.L. Baulch, R.A. Cox, R.F. Hampson Jr., J.A. Kerr and J. Troe, J. Phys. Chem. Ref. Data 21 (1992) 1125.
[30] D.W. Goodman, private communication.
[31] D.N. Belton, C.L. DiMaggio, S.J. Schmieg and K.Y.S. Ng, J. Catal. 157 (1996) 559.
[32] H.J. Borg, J.F.C.-J.M. Reijerse, R.A. van Santen and J.W. Niemantsverdriet, J. Chem. Phys. 101 (1994) 10052.
[33] T.W. Root, G.B. Fisher and L.D. Schmidt, J. Chem. Phys. 85 (1986) 4687.
[34] T.W. Root, L.D. Schmidt and G.B. Fisher, Surf. Sci. 134 (1983) 30.
[35] D.N. Belton, unpublished.